

3D Surface Acquisition for FMT Using High-Accuracy Fringe Projection Profilometry

Seminario ISP
Andrés Marrugo - Feb 2016

3D Surface Acquisition for FMT Using High-Accuracy Fringe Projection Profilometry

Juan E. Ortúñو, Pedro Guerra, *Member, IEEE*, George Kontaxakis, *Senior Member, IEEE*, María J. Ledesma-Carbayo, *Member, IEEE*, and Andrés Santos, *Senior Member, IEEE*

Abstract—An experimental structured light projection system which includes a miniaturized projector is described. The system has been designed to be integrated in a fluorescence molecular tomography (FMT) prototype in order to reconstruct the surface of mice and phantom studies. A high-accuracy phase map is retrieved with phase-shifted sinusoidal fringes. Phase error due to the nonlinear gamma function of the pico-projector is calibrated and compensated. Robust phase unwrapping is performed with an additional Gray-code projection sequence. An automatic phase-to-height non-linear calibration scheme has been applied using objects located in the extremes of the field of view. The accuracy of the proposed method has been tested with a realistic mouse model and ray-tracing software.

of heights relative to the reference plane. The 3D surface can then be reconstructed based on triangulation once the system is properly calibrated.

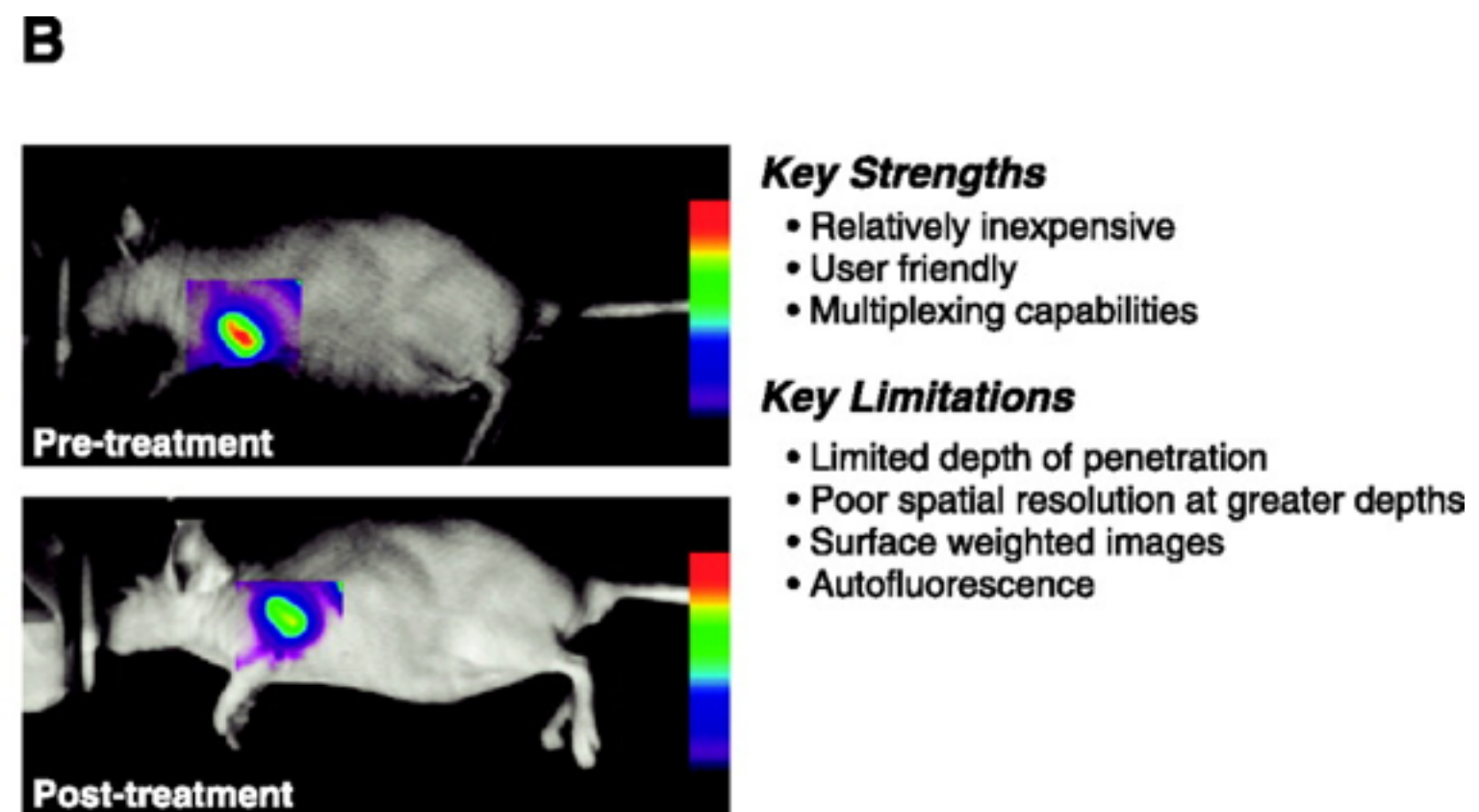
In this paper, we propose the integration of a fringe pattern projection system in a compact FMT prototype using miniaturized digital projectors to acquire the 3D shape of mice and phantom studies.

II. MATERIALS AND METHODS

The structured light projection system has been designed to be integrated in a novel FMT CCD camera based system that

Motivation

Fluorescence Molecular Tomography is an optical imaging technique which aims at reconstructing the **3D distribution of fluorescent markers in bio-tissues** based on surface measurements of emitted photons and a model of light propagation.



[1] M. L. James and S. S. Gambhir, “A Molecular Imaging Primer: Modalities, Imaging Agents, and Applications,” *Physiological Reviews*, vol. 92, no. 2, pp. 897–965, Apr. 2012.

Motivation

- FMT has poor spatial resolution.
- To improve resolution the 3D surface of the mouse is acquired.
 - Sub-millimeter precision is desirable for accurate quantitative measurements.
 - Authors propose integration of fringe projection system with FMT prototype.

[1] M. L. James and S. S. Gambhir, “A Molecular Imaging Primer: Modalities, Imaging Agents, and Applications,” *Physiological Reviews*, vol. 92, no. 2, pp. 897–965, Apr. 2012.

Experimental setup

An experimental setup was mounted to test the proposed code light projection system (Fig. 1) prior to the integration with the FMT prototype. The assembly consists of a low-cost CCD camera (Sony DSC-W1) placed in the top of the device and a pico-projector (model PK101, Optoma Technology, Inc) with DLP® technology (Texas Instruments, Inc.). The pico-projector has a minimum focus range of 210 mm, angular aperture of 35° and HGVA resolution. The setup has dimensions of 20×30×30 cm, appropriate to be further integrated in the FMT prototype, replacing the DSC-W1 camera by the electron-multiplier CCD camera also used to collect fluorescent emissions.

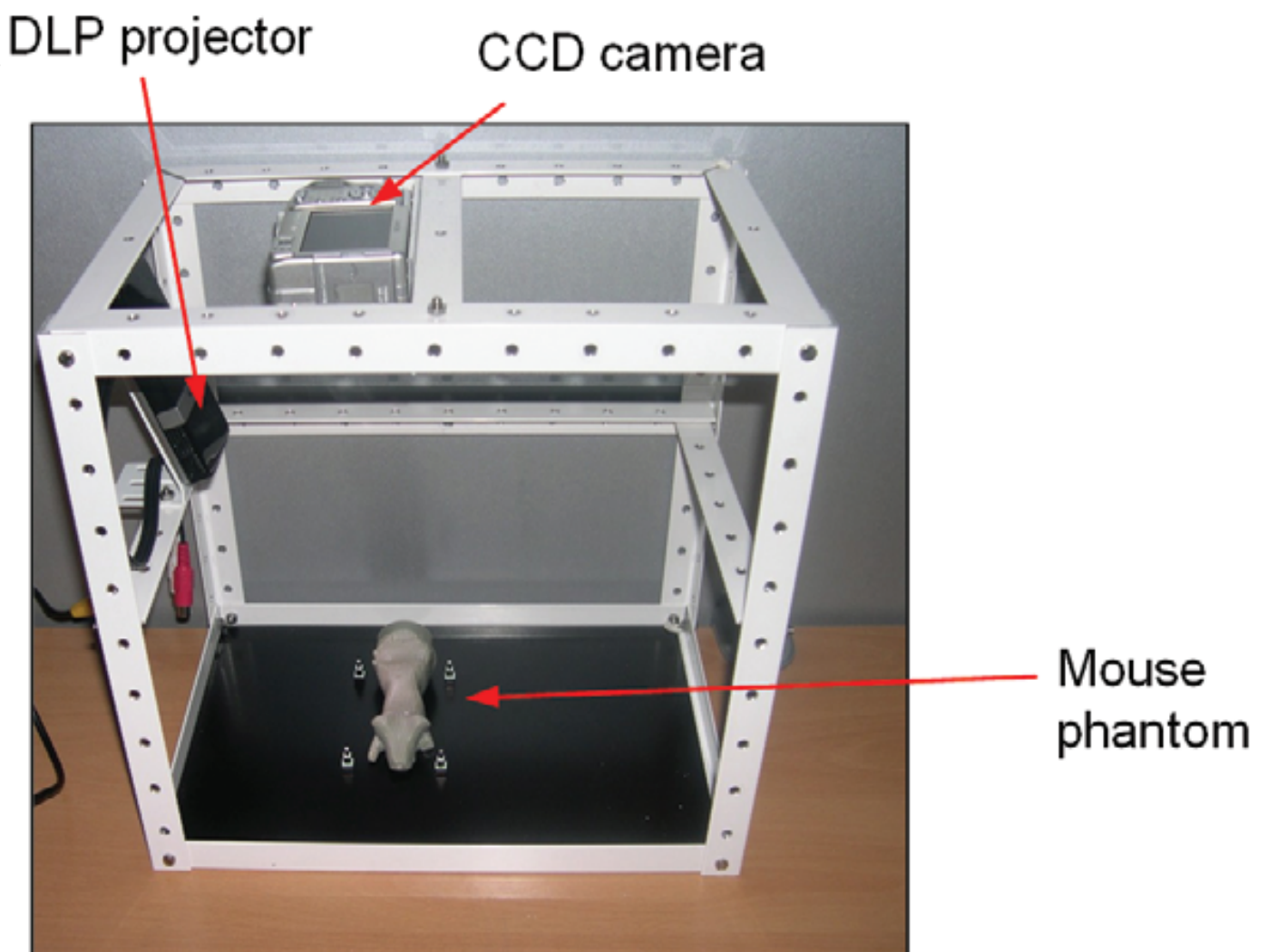


Fig. 1. Experimental setup mounted to test the proposed coded light projection system. The device is composed of a DLP pico-projector and a CCD camera that collects deformed patterns reflected by the object.

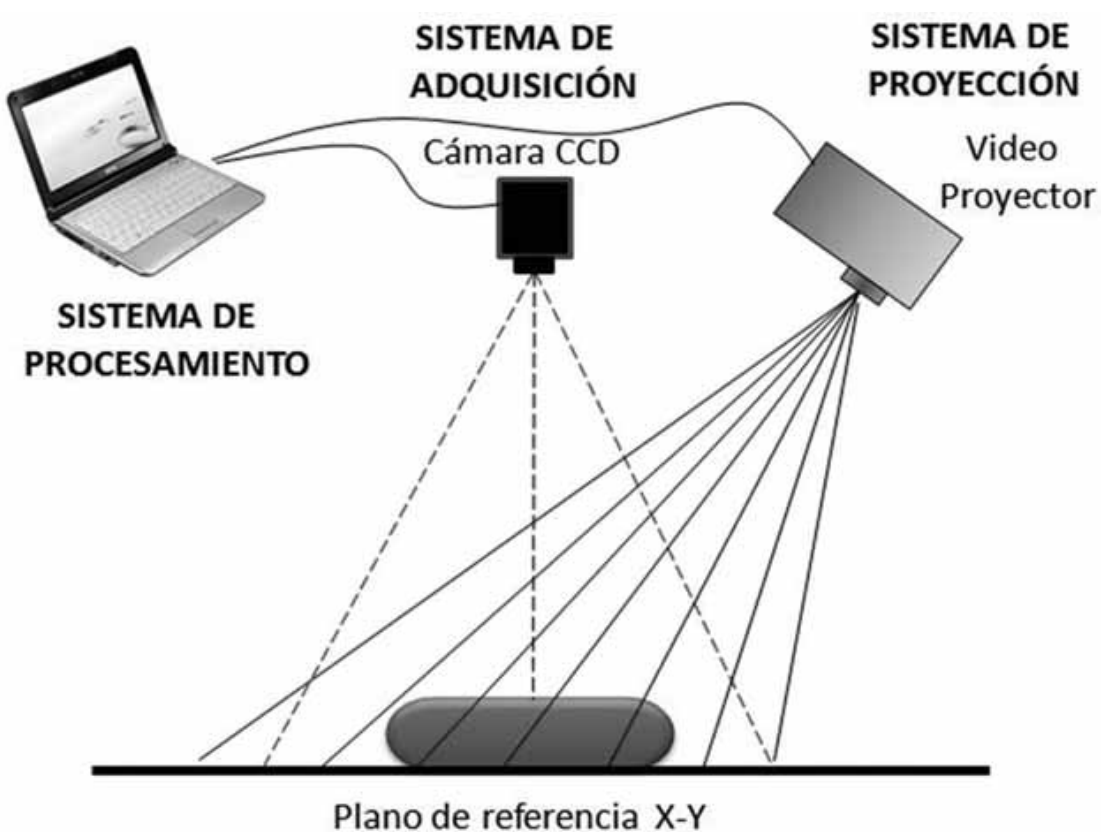
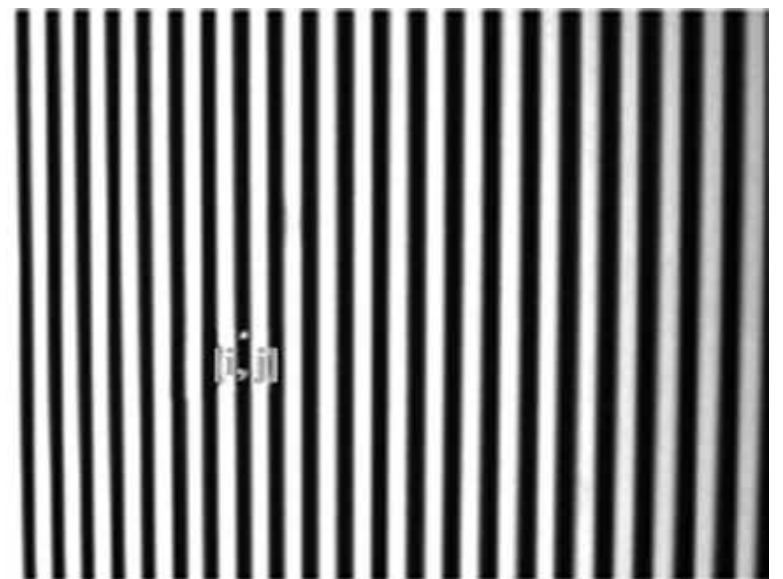
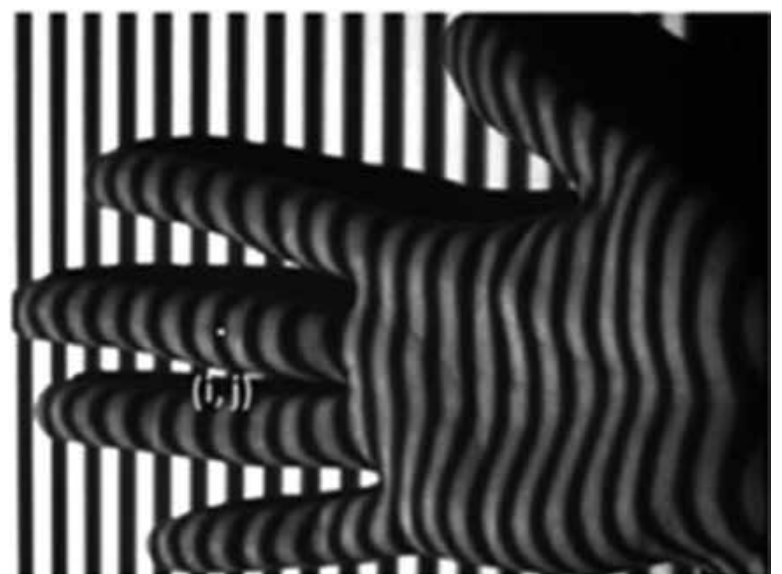


Fig. 1 Montaje experimental de proyección de franjas

$$I(x_o, y_o) = I_0(x_o, y_o) + A(x_o, y_o) * \cos(2\pi f_o x_o + \phi_o)$$



(a)



(b)

Fig. 2 Patrón de franjas proyectado sobre (a) un plano de referencia y (b) mano humana

A. Fringe pattern projections

In each acquisition, four sinusoidal patterns g_i with phase shifts of 90° are projected:

$$g_i(x, y) = a(x, y) + b(x, y) \cos\left(\varphi(x, y) + \frac{\pi}{2} i\right), \quad i = 0, 1, 2, 3 \quad (1)$$

where a is the average intensity and b is the modulation in each point coordinate (x, y) . Wrapped phase φ is solved with:

$$\varphi(x, y) \bmod \pi = \arctan\left(\frac{g_4 - g_2}{g_3 - g_1}\right) \quad (2)$$

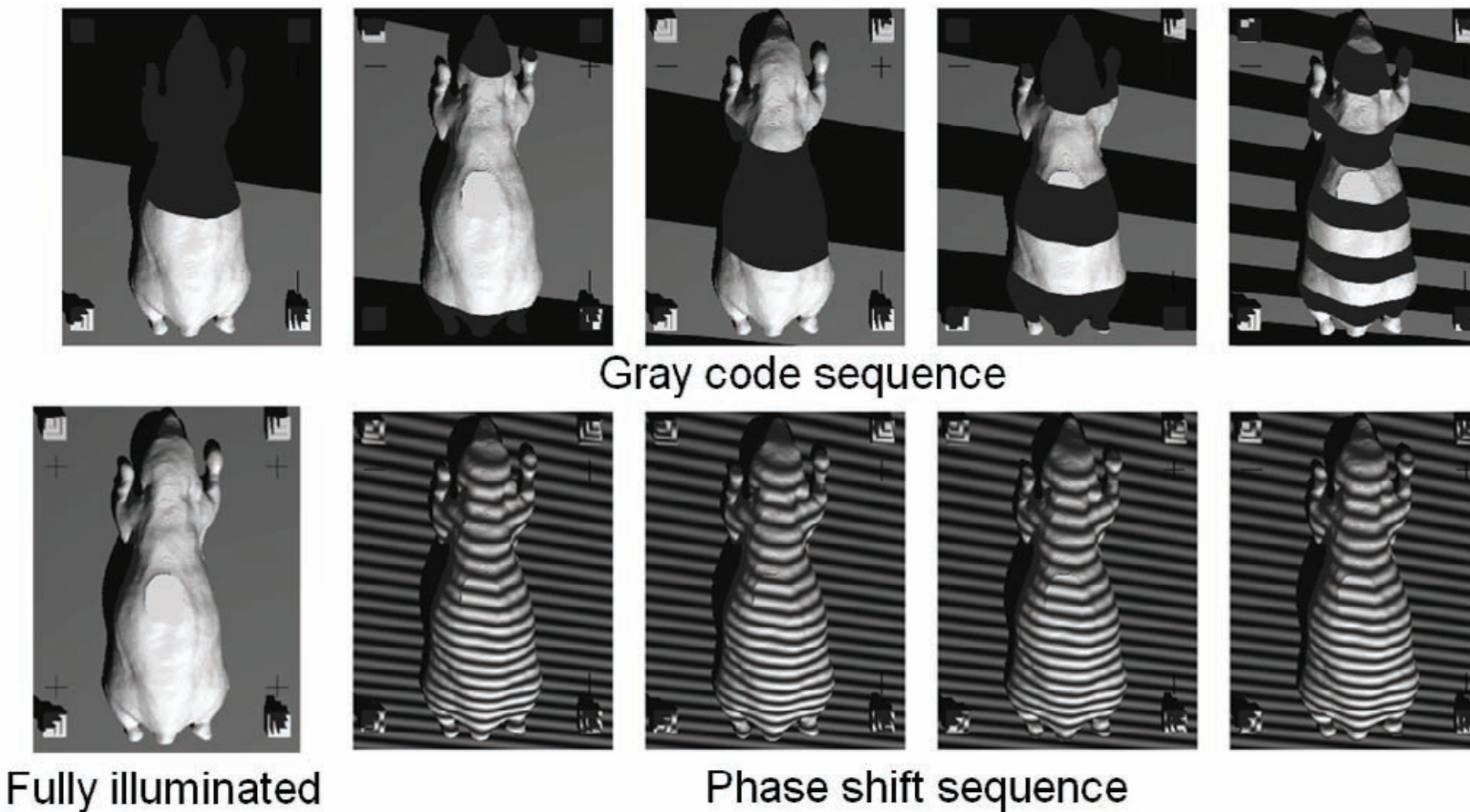


Fig. 2. Ray-tracing simulation of mouse model, showing the structured light patterns.

Phase error due to the gamma function of the DLP projector is compensated with a calibration look-up-table [9]. Phase unwrapping is performed with an additional Gray-code sequence of 5 bits, which is robust to ambiguities in surface discontinuities. The sequence of patterns, including a full illuminated image is shown in Fig. 2 in the case of a Ray-tracing simulation of a mouse model.

Key aspects

- ✓ Phase error due to gamma function of DLP is compensated with calibration look-up table.
- ✓ Phase unwrapping performed with additional Gray-code sequence of 5 bits.
- ✓ Plane of reference in occluded areas (e.g. below mouse) is extrapolated from surrounding values w/ splines.
- ✓ Occluded & shaded zones → 2 acquisitions (2 DLP orientations).
- ✓ Not occluded pixels → mean of 2 acquisitions.
- ✓ Accuracy tested with simulations (POV ray tracing.)

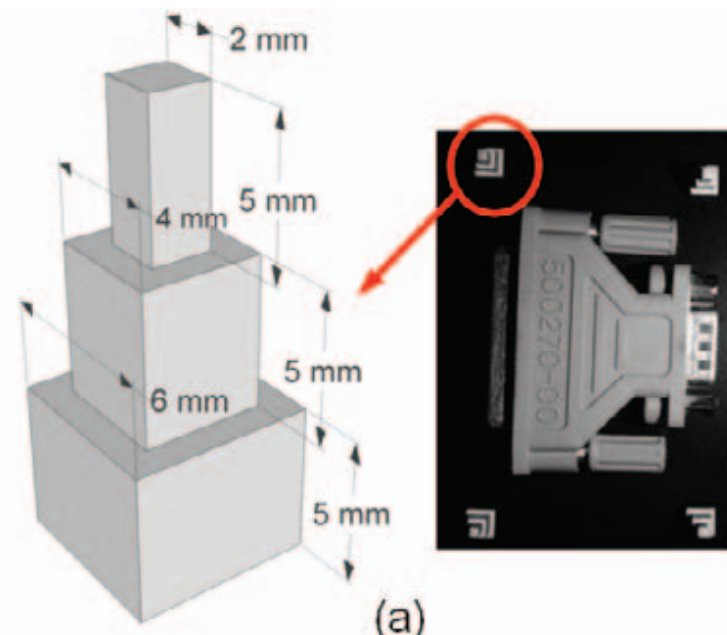
Calibration

- Calibration #1 (non-linear)

tested. Nonlinear phase-to-height mapping [10] is calculated as:

$$h(x,y) = \frac{\Delta\varphi(x,y)}{m(x,y) + n(x,y)\Delta\varphi(x,y)} \quad (3)$$

where $h(x,y)$ is the height over the reference plane in the (x,y) point, $\Delta\varphi$ is the unwrapped phase difference between the object and the reference plane, and (m,n) are the parameters obtained with a least squares minimization algorithm [11]. This calibration procedure, denoted from now on, as calibration #1 for short, requires of the acquisition of at least two planar slabs of different height.



- Calibration #2 (linear)

Linear phase-to-height mapping, denoted from now on as calibration #2, is calculated as:

$$h(x,y) = k(x,y)\Delta\varphi(x,y) \quad (4)$$

In theory, this approach only requires one calibration acquisition to guess the parameter $k(x,y)$. However in practice several measurements are performed to increase the accuracy.

- Calibration #3 (non-linear)

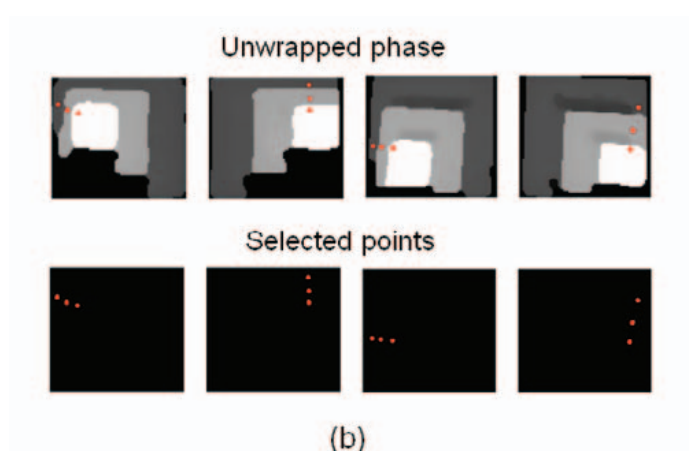


Fig. 3. (a) Stepped pyramid-shaped calibration objects situated together with the object to be measured; (b) detail of unwrapped phase of stepped pyramidal objects and selected points used to non linear calibration marked in red color.

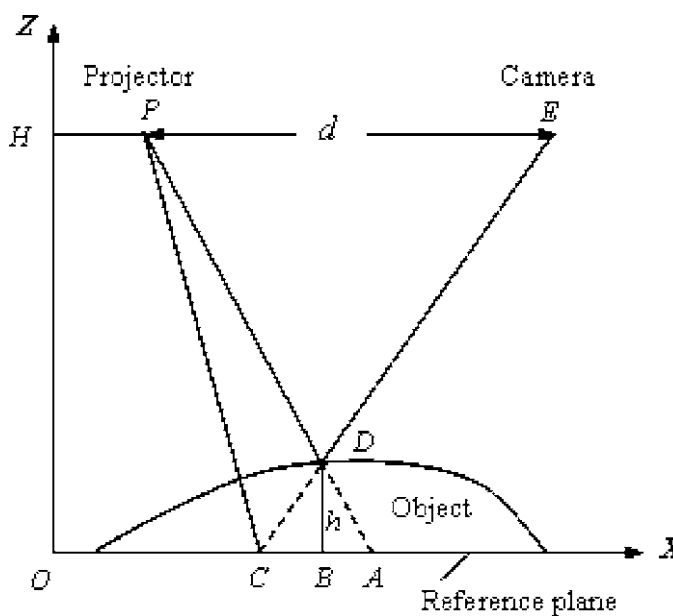


Fig. 2 Relationship between the phase of the projected fringe pattern and the height of the object.

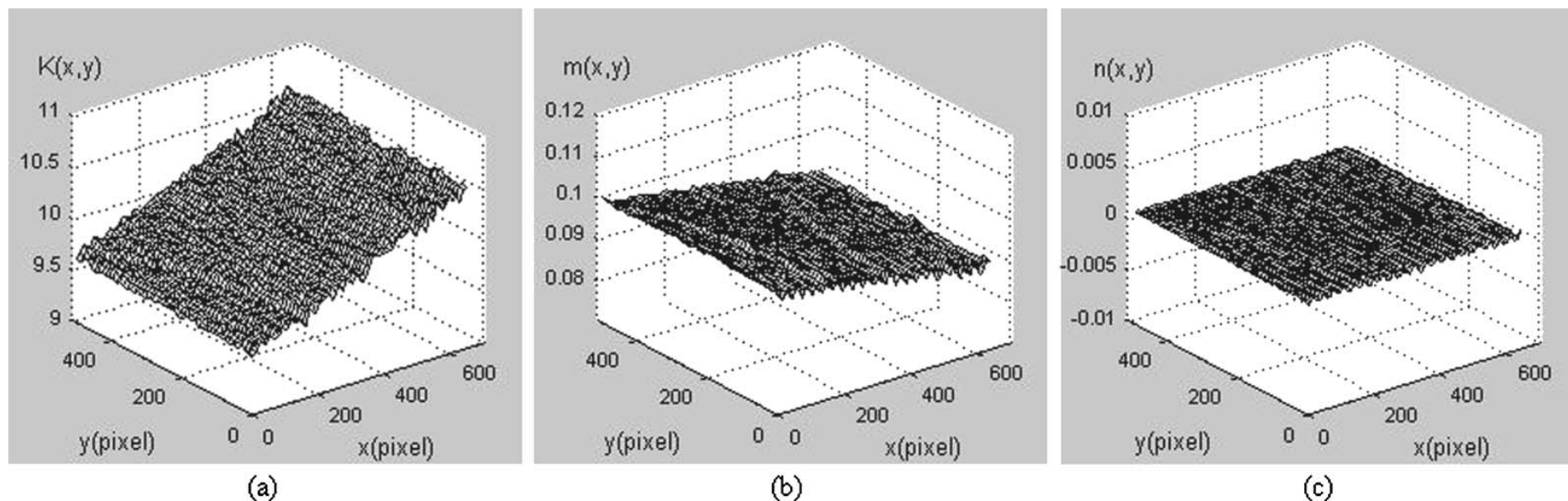
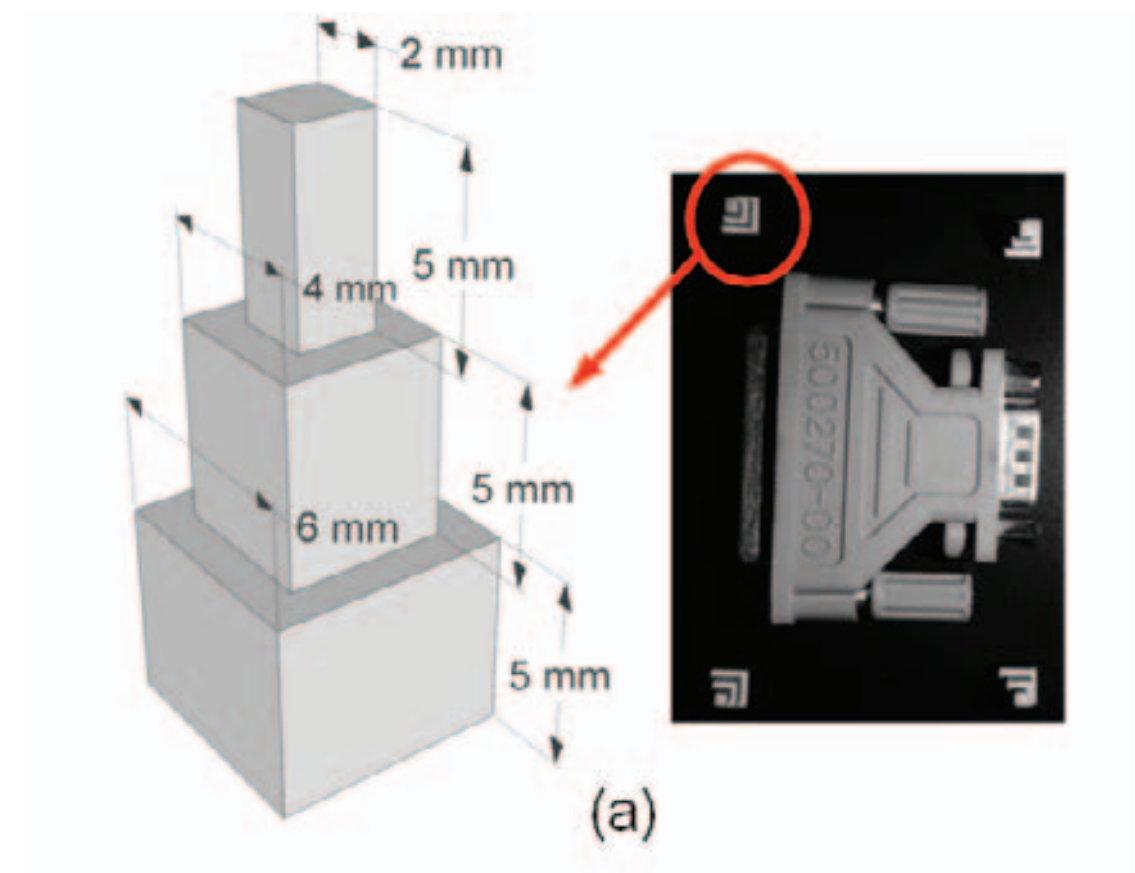


Fig. 4 Results of the real linear and nonlinear calibration: (a) distribution of $K(x,y)$ of the linear calibration; (b,c) distributions of $m(x,y)$ and $n(x,y)$ of the nonlinear calibration.

Calibration

- Calibration #3 assumes non-linear parameters change smoothly.
- Estimation of parameters from 4 points in (x,y) w/ Delaunay Triangulation and polynomial interpolation.



Results

A. Ray-tracing models

Accuracy of the proposed methodology has been tested with simulated acquisitions of a phantom shown in Fig. 4b, composed of 19 steps with height ranges from 1 to 19 mm.

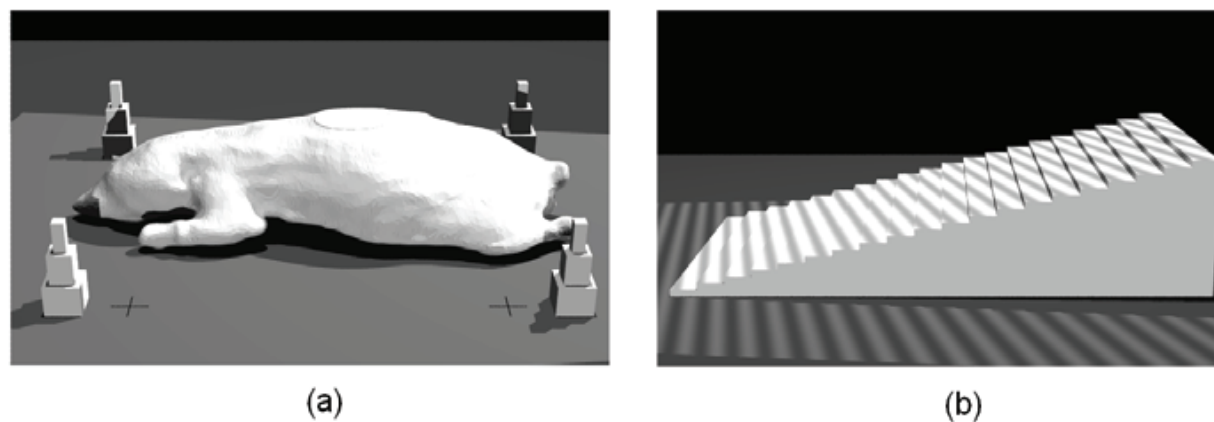


Fig 4. (a) PovRay Rendering of mouse model and stepped pyramid-shaped calibration objects; (b) phantom used to test the accuracy of algorithms, composed of steps of 1 mm height.

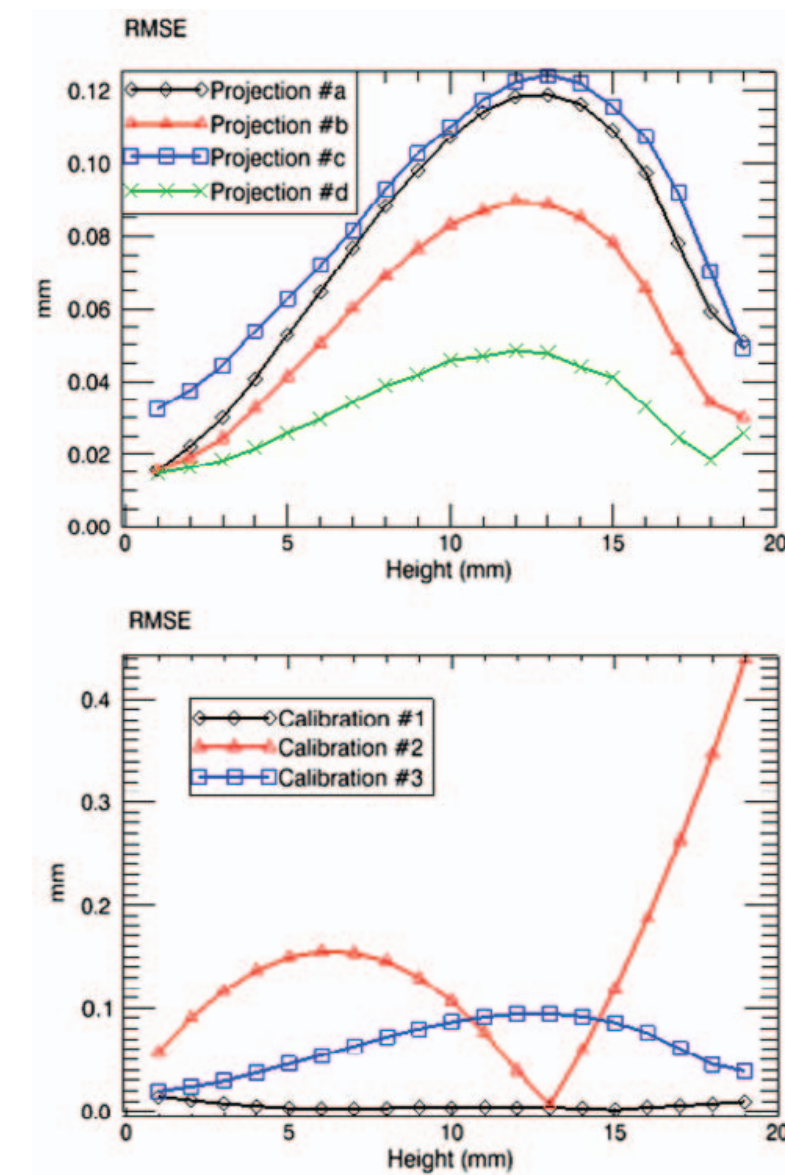


Fig. 5. Upper plot: Root mean square error (RMSE) in four pico-projector locations with nonlinear calibration #3; lower plot: RMSE mean of four pico-projector locations using calibrations #1, #2 and #3.

Results

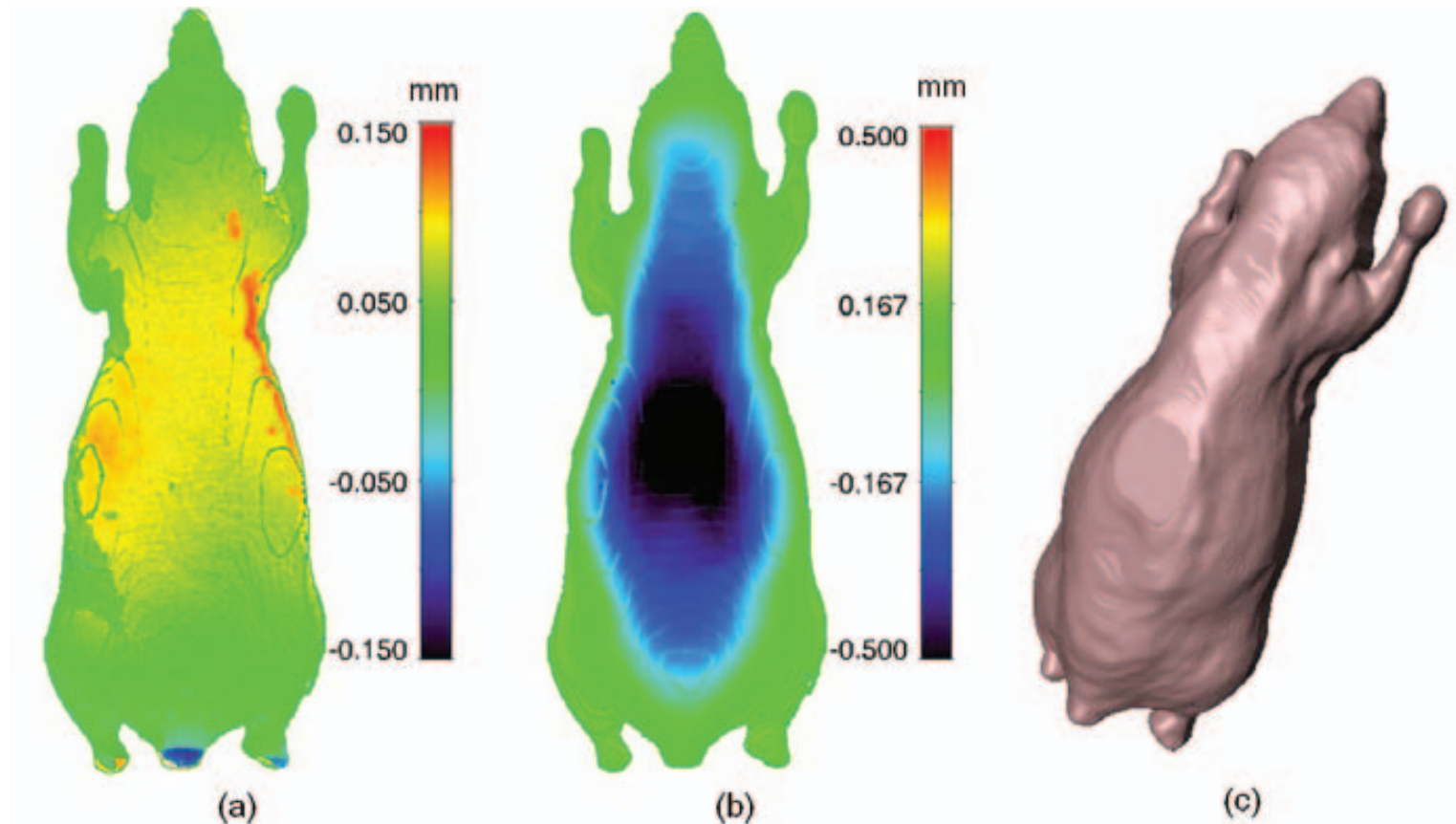


Fig. 6. Mouse surface model: (a) Height difference of calibration #3 with respect to calibration #1; (b) height difference of calibration #2 with respect to calibration #1; (c) rendering of result using calibration #3.

Results

B. Experimental setup

Slabs 4, 8, 12 and 16 mm height were used to calibrate the experimental setup for methods #1 and #2. The acquisitions of these slabs were also employed to evaluate the accuracy of calibration method #3. Table 1 compares the RMSE using calibration #2 and #3.

TABLE 1. HEIGHT ERRORS IN SLABS OF CONSTANT HEIGHT

Height	4 mm	8 mm	12 mm	16 mm
RMSE (μm), method #2	256	215	48	193
RMSE (μm), method #3	76	128	113	99

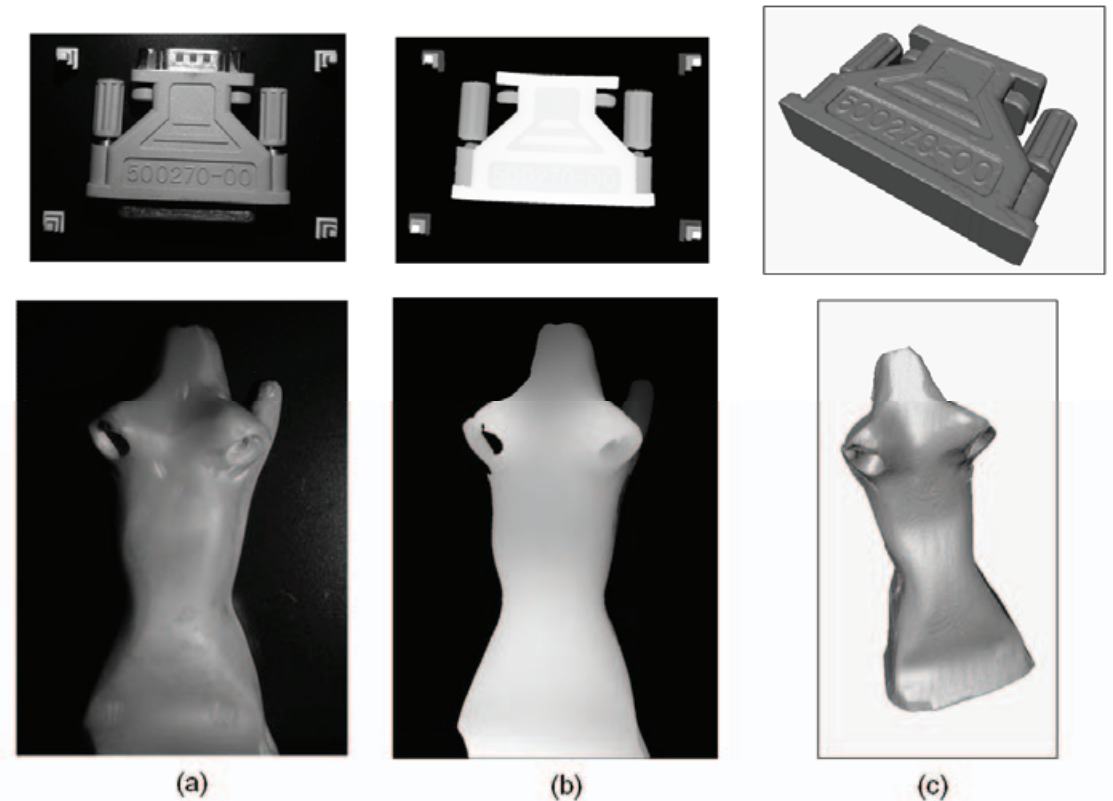


Fig. 7. (a) Full illuminated scene of computer adapter and agar mouse phantom; (b) height map with one projection set. Shaded surfaces are not detected and metallic parts have been eliminated to avoid errors; (c) 3D rendering of reconstructed shapes.